Differential Fed Antenna With High Self-Interference Cancellation for In-Band Full-Duplex Communication System

GIRDHARI CHAUDHARY [ID], **(Member, IEEE), JUNHYUNG JEONG, (Student Member, IEEE), AND YONGCHAE JEONG** [ID], **(Senior Member, IEEE)**

Division of Electronics and Information Engineering, IT Convergence Research Center, Chonbuk National University, Jeonju-si 54896, South Korea

Corresponding author: Yongchae Jeong (ycjeong@jbnu.ac.kr)

ABSTRACT This paper presents a novel design of high self-interference cancellation (SIC) technique for microstrip antennas. The proposed antenna consists of two closely-spaced orthogonal antennas with differential feeding as SIC circuit so as to achieve high interport isolation between the transmitter and receiver. In order to achieve high RF leakage cancellation, a novel differential feeding network (DFN) is also proposed in this paper, which provides amplitude and out-of-phase imbalances within 0.12 ± 0.03dB and $-180 \pm 1°$, respectively, for the bandwidth of 500 MHz at a center frequency of 2.50 GHz. General analytical design equations are derived for achieving high SIC over the wide bandwidth. For experimental validation, prototypes are designed and fabricated at the center frequency of 2.50 GHz using an FR-4 substrate with dielectric constant of 4.4 and loss tangent of 0.02. A good agreement is observed among the theoretical analysis, and the simulation and measurement results. The first fabricated prototype provides more than 64 dB SIC for the bandwidth of 110 MHz, while the second prototype achieved more than 60 dB SIC for 160 MHz bandwidth. In addition, the SIC of the antenna using the proposed DFN is high over the wideband frequency bandwidth as compared to conventional 180° ring hybrid feeding network. Due to ease of implementation and excellent performances, the proposed antennas have potential application for wideband in-band full duplex systems.

INDEX TERMS Analog cancellation, differential feeding network, high RF isolation, passive suppression, in-band full duplex (IBFD), wideband self-interference cancellation (SIC).

I. INTRODUCTION

In-band full duplex (IBFD) system, which can simultaneously transmit and receive a signal over the same time and frequency, has been widely investigated in recent years [1]–[4]. Since IBFD has the theoretical ability to double data through puts and spectral efficiency, the IBFD system is also considered as one of the candidate for a next-generation 5G communication systems to tackle data traffic demand [1]. The major challenge for implementing IBFD systems is reducing the strong self-interference (SI) imposed on the received (RX) signals by the transmitted (TX) signals. The amount of

self-interference cancellation (SIC) depends on the TX signal power, signal bandwidth, and the noise at receiver [1]–[4].

In order to realize advantages of the IBFD system, the SI signal level should be reduced to the same level as the receiver noise. In recent years, a lot of research has gone toward different SIC techniques to achieve desired cancellation [5]–[8]. Based on literature reviews, SIC can be achieved in three domains: TX-to-RX air interface (multiple antennas, circulators, and duplex filters), cancellation in the RF and analog front end, and digital cancellation [9]–[12]. In addition, the SIC should achieve higher than 50 dB in TX-to-RX air interface domain or RF analog stage in order to suppress TX SI (including intermodulation, TX circuit noise, and phase noise) as well as prevent the saturation of the receiver building blocks (low noise amplifier, mixer, and ADC).

The SIC technique at the antenna stage is the first step to achieve high levels of SIC, which can prevent saturation of the receiver. In addition, high SIC at the antenna stage makes other stage cancellations easier without the need for complex RF analog and digital domain techniques [13].

For achieving high isolation at the antenna stage, additional structures on the antenna can be introduced to suppress surface waves or alter ground plane currents, such as bandgap structures, wavetraps, and a slot on the ground plane [14]. However, these techniques are complicated and no accurate calculation methods are applicable to them to achieve high isolation.

Another approach is to make use of orthogonal polarization to obtain high isolation between TX and RX [15]. However, orthogonal polarization is usually not sufficient to ensure the required isolation, because the antennas can generate cross-polarized fields. Similarly, a dual-polarized antenna with a differential feeding network (DFN) in monostatic configuration (same TX and RX antenna) can lead to the improved TX-to-RX interport RF isolation [16]–[18]. In [16], a dual-polarized patch antenna is presented using a DFN that consists of a power divider with two meandering strips with a 180° phase difference to achieve 40 dB isolation between TX and RX ports. Similarly, a dual-polarized patch antenna with the hybrid ring feeding is present in [17], which provides measured isolation of more than 40 dB. In [18], a patch antenna is fed from the same edge where the dual-polarization is obtained by differential excitation of the two side ports with 180° ring hybrid. However, the achievable isolation is limited in this antenna because of strong coupling between the close-spaced microstrip feeding the radiating patch from the same edge. Furthermore, the dual-polarized patch antennas with differential feeding are presented in [19], [20] based on three and four ports, respectively. Although high isolation is obtained in these works, the bandwidth is still limited to 50 MHz at 2.4 GHz center frequency. In addition, the conventional DFNs (such as 180° ring hybrid and Wilkinson power divider (WPD) with unequal microstrip lines) can provide the perfect amplitude balance of 0 dB and phase balance of 180° only at the center frequency, which can limit RF leakage cancellation over a wide bandwidth.

To realize practical high isolation for IBFD system, a bistatic configuration (separate TX and RX antenna) can be implemented at expense of increased system size. Different techniques such as polarization diversity, spatial duplexing, null placement, near field cancellation and feed-forward cancellation were proposed in bistatic configuration to achieve interport isolation [21]–[29].

In this paper, orthogonal polarized antenna with differential feeding in bistatic configuration is demonstrated for IBFD system. To achieve high TX-to-RX port isolation over wide bandwidth in the proposed antenna, a novel DFN is proposed, which provides good amplitude and phase imbalances over wide frequency bandwidth. The accurate design equations are also derived so as to assist with and achieve RF leakage cancellation over the wide frequency bandwidth.
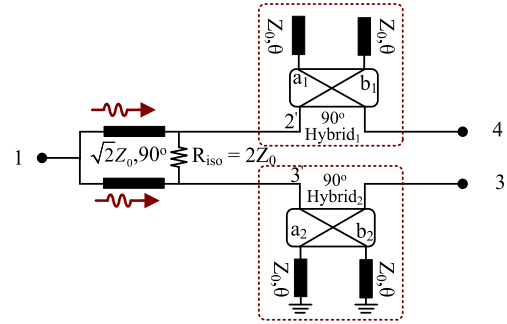
FIGURE 1. Structure of wideband differential feeding network.

II. ANALYTICAL ANALYSIS

A. WIDEBAND DIFFERENTIAL FEEDING NETWORK

Fig. 1 shows the structure of the wideband DFN, which consists of WPD and two 3-dB hybrids. The coupled and through ports of one hybrid are terminated with open-circuited transmission lines (TLs), whereas those of another hybrid are terminated with short-circuited TLs. Assuming the characteristics impedance and electrical lengths of the open and short-circuited TLs are Z_0 and θ, respectively, the S-parameters of the proposed feeding network through different transmission paths can be derived as (1).

$$S_{41}^{DFN}(f) = \left\{ \begin{array}{c} 2S_{2'1}^{W}(f)\, S_{2'a_1}^{H_1}(f)\, S_{2'b_1}^{H_1}(f) \\ e^{-j\left(\varphi_{2'a_1}^{H_1}(f)+\varphi_{2'b_1}^{H_1}(f)+\varphi_{2'1}^{W}(f)\right)} \Gamma_o \end{array} \right\} \quad (1a)$$

$$S_{31}^{DFN} = \left\{ \begin{array}{c} 2S_{3'1}^{W}(f)\, S_{3'a_2}^{H_2}(f)\, S_{3'b_2}^{H_2}(f) \\ e^{-j\left(\varphi_{3'a_2}^{H_2}(f)+\varphi_{3'b_2}^{H_2}(f)+\varphi_{3'1}^{W}(f)\right)} \Gamma_s \end{array} \right\} \quad (1b)$$

where

$$\Gamma_o = e^{-j2\theta(f)} \quad (2a)$$

$$\Gamma_s = e^{-j(\pi+2\theta(f))} \quad (2b)$$

and $S_{ii}^{W}(f)$, $S_{ii}^{H_i}(f)$ are the transmission S-parameters of power divider and hybrids, respectively.

Furthermore, the amplitude and out-of-phase balances between two paths can be written as (3).

$$\Delta_{DFN}(f)) = \left| \frac{S_{31}^{DFN}(f)}{S_{41}^{DFN}(f)} \right| = \left| \frac{S_{3'1}^{W}(f)\, S_{3'a_2}^{H_2}(f)\, S_{3'b_2}^{H_2}(f)}{S_{2'1}^{W}(f)\, S_{2'a_1}^{H_1}(f)\, S_{2'b_1}^{H_1}(f)} \right|$$
$$(3a)$$

$$\Delta\varphi_{DFN}(f) = \angle S_{41}^{DFN} - \angle S_{31}^{DFN}$$
$$= \pi + \left(\begin{array}{c} \varphi_{3'a_2}^{H_2}(f) + \varphi_{3'b_2}^{H_2}(f) - \varphi_{2'a_1}^{H_1}(f) \\ -\varphi_{2'b_1}^{H_1}(f) + \varphi_{2'1}^{W}(f) - \varphi_{3'1}^{W}(f) \end{array} \right)$$
$$= \pi + \left(\Delta\varphi^{H_2}(f) - \Delta\varphi^{H_1}(f) + \Delta\varphi^{W}(f) \right) \quad (3b)$$

As noted from (3), if WPD and both hybrids have perfect amplitudes and phase balances, and both hybrids are identical, then the amplitude and out-of-phase balances of the

overall feeding network can be derived as (4)

$$\Delta_{DFN}(f) = 1 \tag{4a}$$

$$\Delta\varphi_{DFN}(f) = \angle S_{41}^{DFN} - \angle S_{31}^{DFN} = \pi \tag{4b}$$

From (4), it can be concluded that the proposed DFN can theoretically provide perfect amplitude and phase balances of 180° for infinite bandwidth. However, the performance of the WPD and two hybrids characteristics can limit the performance of the feeding network. Therefore, a WPD and hybrids with good amplitude and phase balance over wideband should be chosen in the design process.

Fig. 2 shows the ideal calculated response of DFNs. As shown in the figure, the conventional DFNs such as 180° ring hybrid and WPD with unequal lengths can provide the perfect amplitude balance of 0 dB and phase balances of 180° only at the center frequency (f_0) of 2.5 GHz. However, the amplitude and out-of-phase balances are independent of frequency and only provide infinite theoretical bandwidth in the proposed DFN.
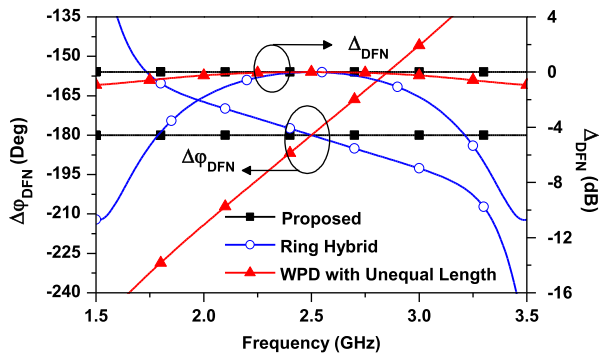
FIGURE 2. Ideal response of different differential feeding networks.

B. WIDEBAND HIGH SIC IN-BAND FULL DUPLEX ANTENNA

Fig. 3 shows the proposed structure of the IBFD antenna with wideband high isolation between the TX and RX ports. The structure consists of circular patch differential fed TX- and single-ended RX-antennas which are orthogonally polarized and closely-spaced. The TX-antenna is excited by the proposed wideband DFN, whereas the RX-antenna is excited with a single-ended co-axial feed network. Signal flow analysis is performed to derive the TX-to-RX isolation by accounting for all coupled signals from TX-to-RX paths. First, the input TX-signal is divided into two out-of-phase signals defined (5) due to DFN.

$$S_1(f) = \frac{S_{41}^{DFN}(f) e^{-j\varphi_{41}^{DFN}(f)}}{\sqrt{2}} \tag{5a}$$

$$S_2(f) = \frac{S_{31}^{DFN}(f) e^{-j(\varphi_{31}^{DFN}(f) + \pi)}}{\sqrt{2}} \tag{5b}$$

Secondly, the leakage signals generated from closely-spaced orthogonal polarized TX-RX antennas will couple with the

outputs of DFN signals. Finally, these leakage signals will be received by the RX antenna. Therefore, TX-to-RX isolation can be determined as in (6).

$$\Delta_{ISO}^{TX-RX} = \frac{1}{S_1(f) \times S_{24}^A(f) e^{-j\varphi_{22}^A} + S_2(f) S_{23}^A(f) e^{-j\varphi_{23}^A}}, \tag{6}$$

where $S_{ij}^A(f)$ and $\varphi_{ij}^A(f)$ are closely-spaced orthogonal polarized antennas leakage signal magnitude and phase, respectively. Using (5) and (6), the TX-to-RX isolation can be further simplified as (7).

$$\Delta_{ISO}^{TX-RX}$$
$$= \frac{\sqrt{2}}{S_{IL}^{DFN}(f) S_{path}^A(f)} \begin{bmatrix} 1 + \{\Delta_{err}^{DFN}(f)\}^2 \{\Delta_{err}^A(f)\}^2 \\ -2\Delta_{err}^{DFN}(f) \Delta_{err}^A(f) \\ \cos\{\Delta\varphi_{err}^{DFN}(f) + \Delta\varphi_{err}^A(f)\} \end{bmatrix}^{-0.5} \tag{7}$$

where amplitude and out-of-phase balance errors of DFN and antenna leakage signals, respectively, are defined by (8).

$$\Delta_{err}^{DFN}(f) = \frac{S_{31}^{DFN}(f)}{S_{41}^{DFN}(f)} \tag{8a}$$

$$\Delta_{err}^A(f) = \frac{S_{23}^A(f)}{S_{24}^A(f)} \tag{8b}$$

$$\Delta\varphi_{err}^{DFN}(f) = \varphi_{31}^{DFN}(f) - \varphi_{41}^{DFN}(f) \tag{8c}$$

$$\Delta\varphi_{err}^{DFN}(f) = \varphi_{23}^A(f) - \varphi_{24}^A(f) \tag{8d}$$

Similarly, $S_{IL}^{DFN}(f)$ and $S_{path}^A(f)$ represent insertion and path losses of DFN and closely spaced orthogonal polarized antennas, respectively. Assuming the DFN is lossless, (7) can be further simplified as (9).

$$\Delta_{ISO}^{TX-RX}$$
$$= \frac{\sqrt{2}}{S_{path}^A(f)} \begin{bmatrix} 1 + \{\Delta_{err}^{DFN}(f)\}^2 \{\Delta_{err}^A(f)\}^2 \\ -2\Delta_{err}^{DFN}(f) \Delta_{err}^A(f) \cos \begin{Bmatrix} \Delta\varphi_{err}^{DFN}(f) \\ +\Delta\varphi_{err}^A(f) \end{Bmatrix} \end{bmatrix}^{-0.5} \tag{9}$$

As shown in (9), the TX-to-RX isolation depends on the amplitude and out-of-phase balance errors of DFN and antenna leakage signals as well as the path loss between the closely-spaced orthogonal polarized antennas. From (9), it can also be noted that the proposed IBFD antenna will provide the infinite TX-to-RX isolation if conditions (10a) and (10b) are both satisfied.

$$\Delta\varphi_{err}^{DFN}(f) = -\Delta\varphi_{err}^A(f) \tag{10a}$$

$$\Delta_{err}^{DFN}(f) = \frac{1}{\Delta_{err}^A(f)} \tag{10b}$$

These conditions for obtaining high isolation between TX-to-RX show that not only are the amplitude and out-of-phase imbalance errors of DFN important but so are those of antenna leakage signals important. Since antenna leakage amplitude and phase balance errors change according to environmental factors, the proposed design equations can
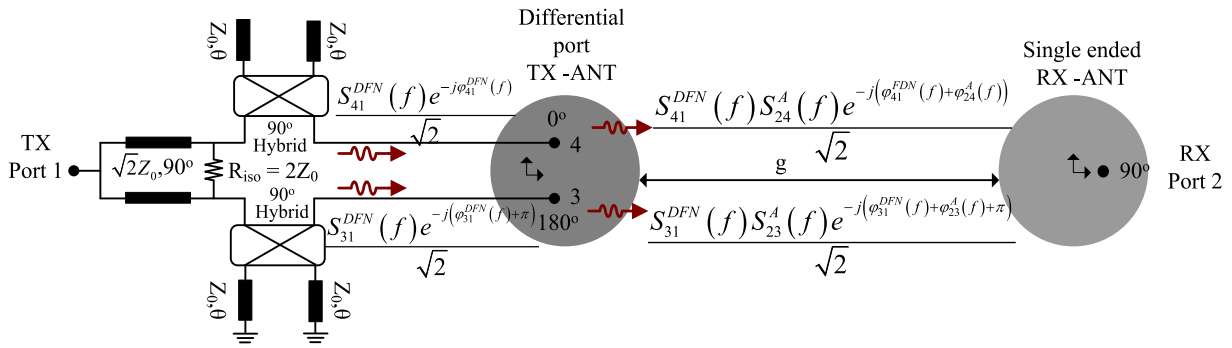
FIGURE 3. The proposed structure of in-band full duplex antenna with wideband high isolation between TX and RX.
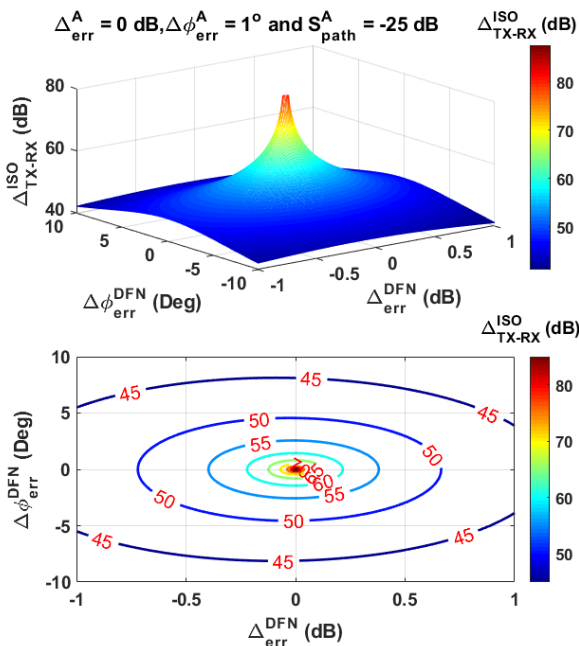
FIGURE 4. TX-to-RX isolation for different amplitude and out-of-phase imbalance errors of DFN with fixed amplitude, phase balance errors of antenna leakage signal and path loss.
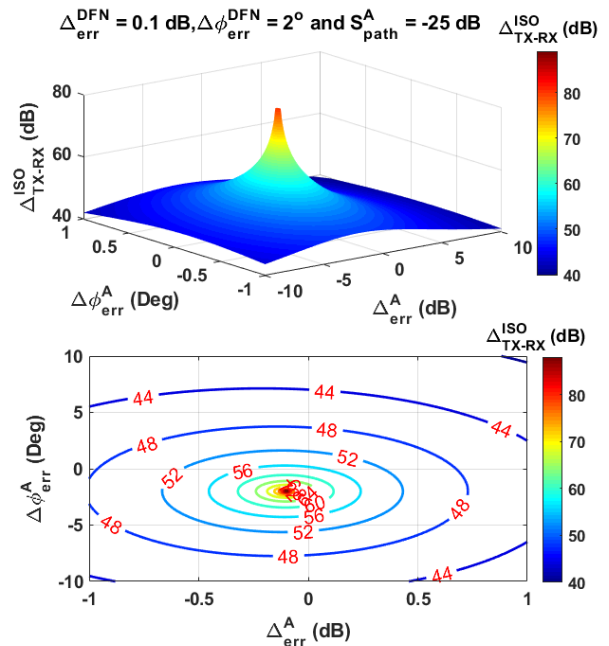
FIGURE 5. TX-to-RX isolation for different amplitude and out-of-phase imbalance errors of antenna leakage signal when the amplitude and out-of-phase balance errors of DFN are fixed.

assist the adaptation of high isolation in the IBFD antenna. Moreover, additional circuits (such as attenuator and phase shifter) can be utilized at the arm(s) of DFN for automatic tuning.

In order to validate the analytical equations, Figs. 4 and 5 show the calculated TX-to-RX isolation of IBFD antenna under different parameters variation. As observed from these figures, the high TX-to-RX isolation over wide frequency bandwidth can be achieved if conditions (10a) and (10b) are both satisfied in terms of overall frequency bandwidth.

In addition, the TX-to-RX isolation higher than 60 dB can be achieved if the amplitude and out-of-phase imbalance errors of DFN and antenna leakage signals are maintained within 0.2 dB and 2°, respectively.

III. SIMULATION AND MEASUREMENT RESULTS
The For experimental demonstration, the DFN and antennas are fabricated at the center frequency of 2.5 GHz using an FR-4 substrate with a dielectric constant of 4.4 and loss tangent of 0.02.

A. RESULTS OF WIDEBAND DIFFERENTIAL FEEDING NETWORK
Fig. 6 shows the physical layout and fabricated photograph of the wideband DFN. The proposed DFN is simulated and fabricated using 3-dB hybrids from ANAREN in FR-4 substrate with a thickness of 1.2 mm. The amplitude and phase errors of 3-dB hybrids are within ±0.4 dB and 90±2° for 2–3 GHz. The physical dimensions of the overall feeding network are also shown in Fig. 6.
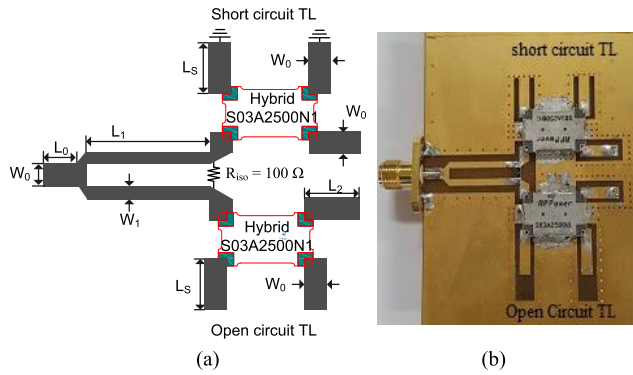
FIGURE 6. (a) Physical layout and (b) photograph of fabricated DFN using FR4-substrate. Physical dimensions: $W_0 = 2.3$, $W_1 = 1.4$, $L_0 = 5$, $L_1 = 16.4$, $L_2 = 8.6$, $L_S = 8$. Unit: mm.
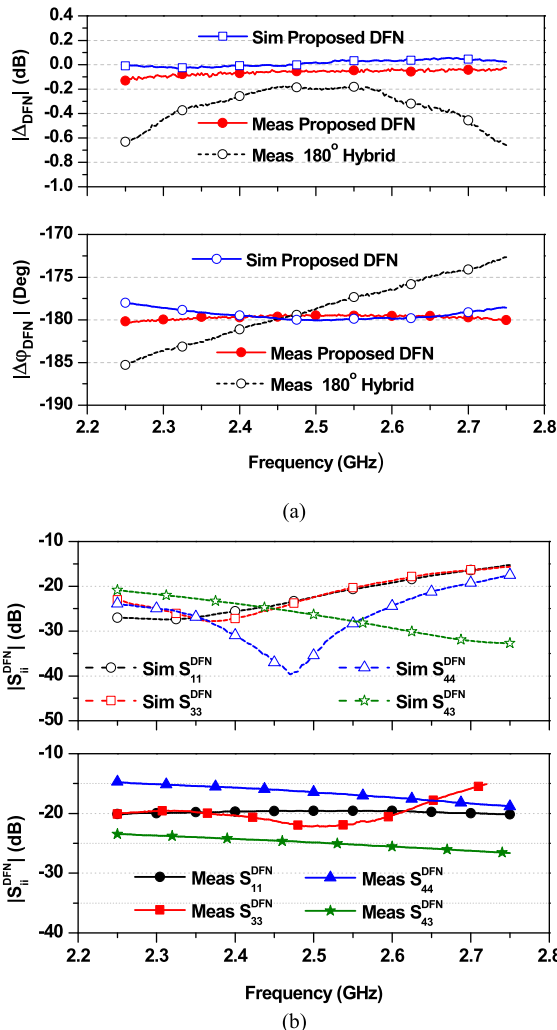
FIGURE 7. Simulated and measured results of the differential feeding network: (a) magnitudes/phase characteristics and (b) return loss/isolation characteristics.

Fig. 7 (a) shows the simulation and measurement results of the DFN networks. From the experiment, Δ_{DFN} and $\Delta\varphi_{\text{DFN}}$ of the proposed DFN are determined to be 0.063 dB and
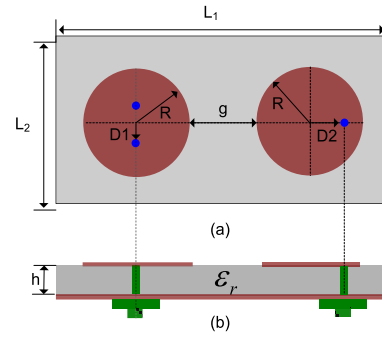
FIGURE 8. Physical layout of closely spaced orthogonal polarized circular patch antenna: (a) top view and (b) side view.
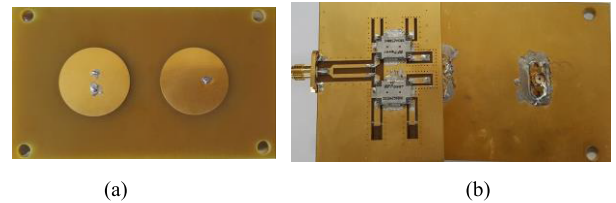
FIGURE 9. Photographs of fabricated in-band full duplex antenna: (a) top view and (b) a bottom view.

$-179.8°$ at $f_0 = 2.50$ GHz, respectively. Similarly, the Δ_{DFN} and $\Delta\varphi_{\text{DFN}}$ are 0.12 ± 0.03 dB and $-180° \pm 1.1°$ within the bandwidth of 500 MHz, respectively. However, Δ_{DFN} and $\Delta\varphi_{\text{DFN}}$ of the conventional 180° ring hybrid are 0.45 ± 0.25 dB and $-180° \pm 5°$, respectively. In addition, the $\Delta\varphi_{\text{DFN}}$ of the conventional feeding network is exactly 180° only at the center frequency.

Fig. 7 (b) shows the simulated and measured return losses and isolation between the output ports of the DFN. From the measurement results, it is found that the input/output return losses and the isolation between output ports are higher than 15.5 dB and 24 dB within the bandwidth of 500 MHz, respectively.

B. PROTOTYPE I: RESULTS OF WIDEBAND HIGH TX-RX ISOLATION IN-BAND FULL DUPLEX ANTENNA

For an experimental demonstration of the proposed IBFD antenna, prototype-I is designed and fabricated at $f_0 = 2.50$ GHz with FR-4 substrate and thickness of 3.2 mm. The upper layer circular patches operate at 2.5 GHz with an orthogonal linear polarization which is placed closely within $0.1\lambda_0$ spacing (λ_0 is the free-space wavelength at 2.50 GHz).

The physical dimensions of the fabricated antenna shown in Fig. 8 and 9 are summarized as: $h = 3.2$, $L_1 = 128$, $L_2 = 72$, $R = 16$, $D_1 = 4$, $D_2 = 5$, and $g = 10$ (all units in mm). In this work, the closely-spaced TX- and RX-antennas with orthogonally polarization structures are chosen so as to obtain leakage isolations of 25 to 30 dB as maintaining compact circuit size. However, this isolation is far from the requirement of the IBFD system, therefore, additional isolation can be obtained with DFN as shown in Fig. 3.
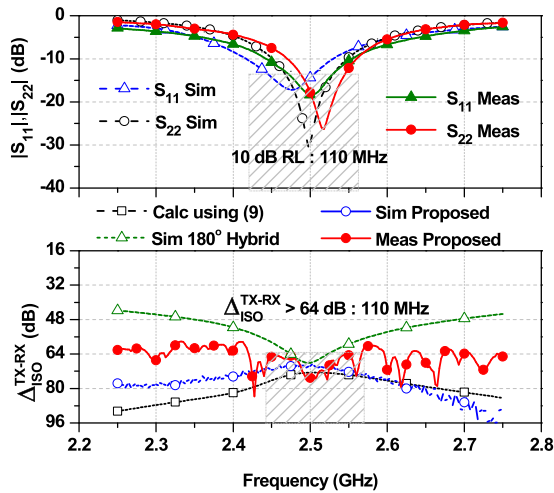
FIGURE 10. Simulated and measured return loss and TX-to-RX isolation of prototype I.

FIGURE 11. Simulated and measured 2-D radiation patterns of the prototype-I antenna in cases of (a) TX-port and (b) RX-port excitations.

FIGURE 12. Measured peak gains of prototype-I.

The antennas are excited through the coaxial feed technique and the DFN is attached at the bottom layer of the TX-antenna with SMA connectors.

Fig. 10 shows the simulated and measured TX and RX-port return losses (RLs) and TX-to-RX isolations of fabricated IBFD antenna prototype-I. The measurements were performed in a laboratory environment and the results were taken directly from a full-assembled antenna system as shown in Fig. 10. The simulation S-parameters results were obtained as follows: First, the 3-D full-wave simulations of circular patch antennas and DFN are performed separately using ANSYS Electromagnetics Suit 19 and the S-parameters are saved as 3-port touchstone files. These touchstones files are imported into circuit simulator advanced design system (ADS) 2017. Finally, the circuit simulations of the entire system are executed, and the results are extracted.

The measured input/output return losses shown in Fig. 10 (a) are slightly deviated from simulation results due to fabrication error. From the experiment, the antenna input/output return losses were higher than 18 dB at $f_0 = 2.52$ GHz. In addition, 10-dB RL bandwidth of the fabricated antenna was determined as 110 MHz. The TX-to-RX isolation of fabricated prototype-I was determined as higher than 70 dB at 2.52 GHz and higher than 64 dB within the bandwidth of 110 MHz. In addition, the measured TX-to-RX isolation is very similar with to the simulated and MATLAB calculated results. Moreover, the TX-to-RX isolation in case of conventional feeding network (180° hybrid) is higher than 64 dB only at f_0.

Fig. 11 (a) shows the simulated and measured 2-D E-plane and H-plane radiation patterns of TX-antenna at $f_0 = 2.50$ GHz. The TX antenna (differential port) is excited while maintaining the RX antenna is loaded with a 50 Ω termination impedance. The measurement was performed at the Korea Electronics Technology Institute (KETI) anechoic chamber. Under TX-port excitation, the maximum radiation was oriented at $\theta = -30°$ with a measured peak gain of 3.75 dBi.
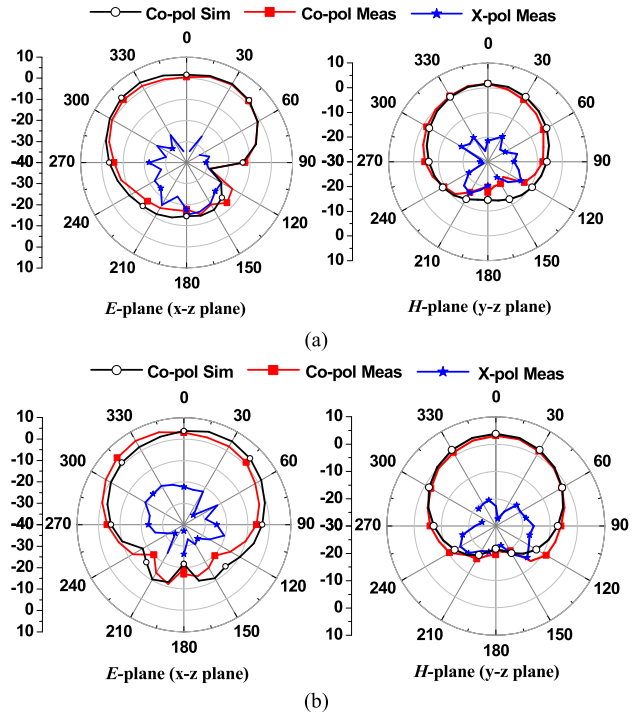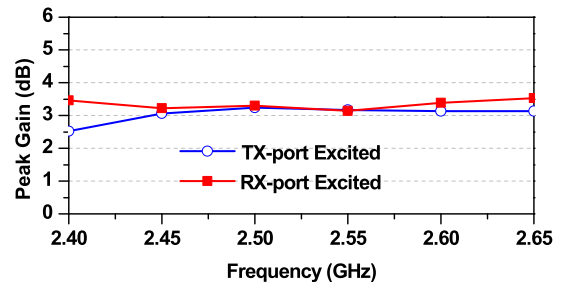
Similarly, Fig. 11 (b) shows the simulated and measured RX antenna 2-D radiation patterns for E-plane and H-plane at $f_0 = 2.50$ GHz. When the RX-port is excited, and the TX-port is loaded with 50 Ω termination, the maximum radiation pattern is oriented at $\theta = -30°$ and $\varphi = 0°$ with a measured peak gain of 3.70 dBi. In addition, the cross-polarization components remain at less than -20 dB for the TX-and RX-antennas.

Fig. 12 shows the measured peak realized gains TX and RX antennas as a function of frequency. The peak gain of TX-antenna is higher than 3.2 dBi, whereas that of RX-antenna is higher than 2.75 dBi within the bandwidth of 100 MHz. As can be seen from these results, the TX-antenna gain is lower than the RX-gain because of the additional insertion loss of DFN in the TX-antenna.

C. PROTOTYPE II: RESULTS OF WIDEBAND HIGH TX-TO-RX ISOLATION IN-BAND FULL DUPLEX ANTENNA

The prototype-I of the proposed IBFD antenna provides high TX-to-RX isolation within 500 MHz bandwidth; however, the 10-dB RL bandwidth of the antenna is only 110 MHz.

Therefore, the second prototype of the IBFD antenna is designed and fabricated by increasing the thickness of the substrate through attaching two units of the FR-4 substrate of thickness 3.2 mm, as shown in Fig. 13. The physical dimensions of prototype II are given as: h = 6.4, L_1 = 124.6, L_2 = 70.3, R = 15.16, D_1 = 4.3, D_2 = 6.2, g = 10 (all units in mm). Fig. 14 shows the photograph of fabricated prototype-II.
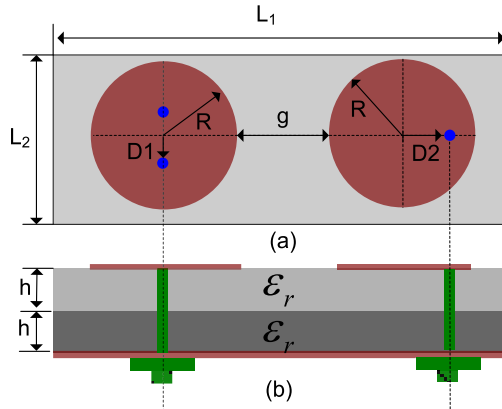
FIGURE 13. Physical layout of a closely spaced orthogonal polarized circular patch antenna with increased substrate thickness: (a) top view and (b) side view.
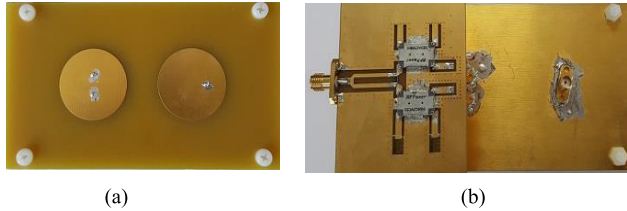
FIGURE 14. Photographs of fabricated prototype-II: (a) top view and (b) a bottom view.

The simulated and measured TX- and RX-port return losses and TX-to-RX isolation are shown in Fig. 15. The measurements were performed in a laboratory environment. As can be seen in the figure, the measured results are consistent with the simulated and theoretically predicted results. The measured TX- and RX-port return losses are higher than 20 dB at f_0 = 2.52 MHz. Similarly, 10-dB RL bandwidth of the prototype-II is determined from the experiment to be 160 MHz, which is wider than that of prototype-I. Similarly, the measured TX-to-RX isolation is higher than 68 dB at f_0 = 2.52 GHz and higher than 60 dB for a bandwidth of 160 MHz. As like prototype-I, the TX-to-RX isolation in case of conventional 180° hybrid feeding network is higher than 65 dB only at center frequency.

Fig. 16 shows the simulated and measured 2D E-plane and $H-$plane gain patterns at 2.50 GHz. As expected, and as is clearly visible from the figure, the maximum TX- antenna gain (when TX-port is excited) of 5.7 dBi is located at $\theta = -30°$, $\varphi = 0°$. Similarly, the maximum RX-antenna gain is
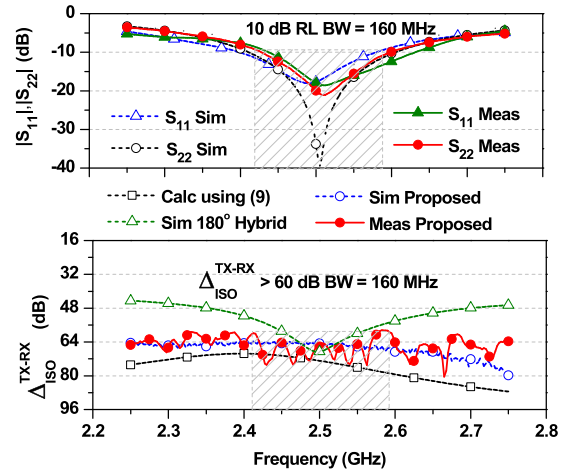
FIGURE 15. Simulated and measured return loss and TX-to-RX isolations of prototype-II.
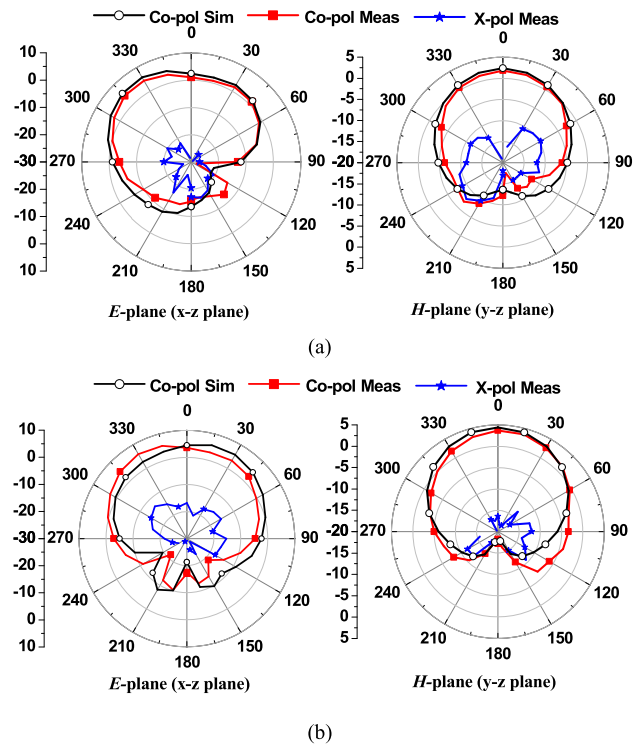
FIGURE 16. Simulated and measured 2-D gain patterns at 2.5 GHz in cases of (a) TX-port and (b) RX- port excitations.

5.72 dBi when the RX-port is excited; which is located at $\theta = -30°$, $\varphi = 0°$. In addition, the TX- and RX-antennas cross polarization components are higher than −20 dB.

Fig. 18 shows the measured peak gains of prototype-II by exciting one port and terminating the other port with 50 Ω. From the measurement, the gain is higher than 4.5 dBi when the TX port is excited, whereas the gain is higher than 5.1 dBi when RX-port is excited within the frequency bandwidth of 160 MHz. The reduction in TX-antenna gain is due to the additional insertion loss of the DFN. The measured radiation

TABLE 1. Performance comparison of the proposed ibfd antennas with state-of-art.

	f_0 (GHz)	10-dB RL BW (dB)	SIC (dB)	SIC BW (MHz)	Spacing between ANT	Overall Antenna Size (Length/Width)	SIC techniques
[21]	4.60	600	50	300	$0.08\lambda_0$	$0.921\lambda_0 \times 0.760\lambda_0$	Polarization diversity
[22]	2.50	220	40	220	$0.10\lambda_0$	$1.081\ \lambda_0 \times 0.750\lambda_0$	Polarization diversity
[24]	0.85	10	25	10	$\approx 0.31\lambda_0$	$0.311\lambda_0 \times 0.155\lambda_0$	Spatial duplexing
[25]	5.80	80	35	80	$0.03\lambda_0$	$0.862\lambda_0 \times 0.580\lambda_0$	ACPS wall
[26]	5.80	270	20	270	$0.07\lambda_0$	$0.881\lambda_0 \times 0.580\lambda_0$	Interdigital lines
[28]	6	50	60	50	NA	NA	Antenna array/DFN
[29]	2.45	300	29.1	300	NA	$1.208\lambda_0 \times 0.857\lambda_0$	Feed-forward
This work I	2.50	110	64	110	$0.08\ \lambda_0$	$1.066\lambda_0 \times 0.6\lambda_0$	DFN
This work II	2.50	160	60	160	$0.08\ \lambda_0$	$1.038\lambda_0 \times 0.585\lambda_0$	DFN

ACPS: Asymmetrical coplanar strip, NA: Dimensions are not provided.
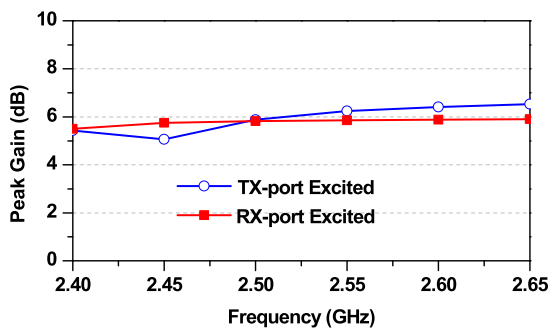
FIGURE 17. Measured peak gains of IBFD antenna prototype II.

efficiencies of TX-and RX-antenna are higher than 58% and 75%, respectively. The radiation efficiency can be further improved by using a low tangent loss substrate.

Table 1 shows the performance comparison of bistatic IBFD antenna in terms of TX-to-RX isolation. As observed in this table, the proposed IBFD antenna provides high SIC between the TX and RX ports as compared to the state-of-the-arts antennae.

IV. CONCLUSION

This work demonstrated the design of an in-band full duplex bistatic antenna with high isolation between transmitting and receiving ports using closely-spaced differential fed circular patch antennas. The novel differential feeding network is also demonstrated with excellent amplitude and phase balance of 180° within 500 MHz bandwidth at center frequency of 2.5 GHz, which can achieve high self-interference cancellation within the wide bandwidth. The general design equations are derived to assist in the design of the wideband high self-interference cancellation full duplex antenna. The fabricated in-band full duplex antennas achieved higher than 60 dB self-interference cancellation within the bandwidth of 160 MHz without any complex circuits, which can make other stage cancellation easier. In addition, the interport isolation of antenna using the proposed differential feeding network is high over wide bandwidth as compared to the conventional 180° hybrid feeding network. The proposed circuit can be further combined with a digital cancellation circuit to achieve the requirement of an in-band full duplex system (such as having higher than 110 dB cancellation). The easy implementation and good performance indicate that the proposed method is a good candidate for wideband in-band full duplex systems.

REFERENCES

[1] S. Hong *et al.*, "Applications of self-interference cancellation in 5G and beyond," *IEEE Commun. Mag.*, vol. 52, no. 2, pp. 114–121, Feb. 2014.

[2] M. Mikhael, B. van Liempd, J. Craninckx, R. Guindi, and B. Debaillie, "An in-band full-duplex transceiver Prototype with an in-system automated tuning for RF self-interference cancellation," in *Proc. 1st Int. Conf. 5G Ubiquitous Connectivity*, Nov. 2014, pp. 110–115.

[3] M. Jain *et al.*, "Practical, real-time, full duplex wireless," in *Proc. 17th Annu. Int. Conf. Mobile Comput. Netw. (MOBICOM)*, New York, NY, USA, Sep. 2011, pp. 301–312.

[4] L. Laughlin, M. A. Beach, K. A. Morris, and J. L. Haine, "Electrical balance duplexing for small form factor realization of in-band full duplex," *IEEE Commun. Mag.*, vol. 53, no. 5, pp. 102–110, May 2015.

[5] D. Bharadia, E. McMilin, and S. Katti, "Full duplex radios," *ACM SIG-COMM Comput. Commun. Rev.*, vol. 43, no. 4, pp. 375–386, Oct. 2013.

[6] M. E. Knox, "Single antenna full duplex communications using a common carrier," in *Proc. IEEE Wireless Microw. Technol. Conf. (WAMICON)*, Apr. 2012, pp. 1–6.

[7] L. Laughlin, C. Zhang, M. A. Beach, K. A. Morris, and J. Haine, "A widely tunable full duplex transceiver combining electrical balance isolation and active analog cancellation," in *Proc. IEEE Veh. Technol. Conf. (VTC Spring)*, May 2015, pp. 1–5.

[8] B. Debaillie *et al.*, "Analog/RF solutions enabling compact full-duplex radios," *IEEE J. Sel. Areas Commun.*, vol. 32, no. 9, pp. 1662–1673, Sep. 2014.

[9] K. E. Kolodziej, J. G. McMichael, and B. T. Perry, "Multitap RF canceller for in-band full-duplex wireless communications," *IEEE Trans. Wireless Commun.*, vol. 15, no. 6, pp. 4321–4333, Jun. 2016.

[10] E. Foroozanfard, O. Franek, A. Tatomirescu, E. Tsakalaki, E. de Carvalho, and G. F. Pedersen, "Full-duplex MIMO system based on antenna cancellation technique," *IET Electron. Lett.*, vol. 50, no. 16, pp. 1116–1117, Jul. 2014.

[11] S. Khaledian, F. Farzami, B. Smida, and D. Erricolo, "Inherent self-interference cancellation for in-band full-duplex single-antenna systems," *IEEE Trans. Microw. Theory Techn.*, vol. 66, no. 6, pp. 2842–2850, Jun. 2018.

[12] E. Ahmed and A. M. Eltawil, "All-digital self-interference cancellation technique for full-duplex systems," *IEEE Trans. Wireless Commun.*, vol. 14, no. 7, pp. 3519–3532, Jul. 2015.

[13] H. Kang and S. Lim, "High isolation transmitter and receiver antennas using high-impedance surfaces for repeater applications," *J. Electromagn. Waves Appl.*, vol. 27, no. 18, pp. 2281–2287, Sep. 2013.

[14] P. Lindberg and E. Ojefors, "A bandwidth enhancement technique for mobile handset antennas using wavetraps," *IEEE Trans. Antennas Propag.*, vol. 54, no. 8, pp. 2226–2233, Aug. 2006.

[15] H. Nawaz and I. Tekin, "Three dual polarized 2.4 GHz microstrip patch antennas for active antenna and in-band full duplex applications," in *Proc. 16th Medit. Microw. Symp. (MMS)*, Nov. 2016, pp. 1–4.

[16] C.-Y.-D. Sim, C.-C. Chang, and J.-S. Row, "Dual-feed dual-polarized patch antenna with low cross polarization and high isolation," *IEEE Trans. Antennas Propag.*, vol. 57, no. 10, pp. 3405–3409, Oct. 2009.

[17] K. Luo, W.-P. Ding, Y.-J. Hu, and W.-Q. Cao, "Design of dual-feed dual-polarized microstrip antenna with high isolation and low cross polarization," *Prog. Electromagn. Res. Lett.*, vol. 36, pp. 31–40, Jan. 2013.

[18] H. Nawaz and I. Tekin, "Compact dual-polarised microstrip patch antenna with high interport isolation for 2.5 GHz in-band full-duplex wireless applications," *IET Microw., Antennas Propag.*, vol. 11, no. 7, pp. 976–981, Jun. 2017.

[19] H. Nawaz and I. Tekin, "Dual-polarized, differential fed microstrip patch antennas with very high interport isolation for full-duplex communication," *IEEE Trans. Antennas Propag.*, vol. 65, no. 12, pp. 7355–7360, Dec. 2017.

[20] H. Nawaz and I. Tekin, "Double-differential-fed, dual-polarized patch antenna With 90 dB interport RF isolation for a 2.4 GHz in-band full-duplex transceiver," *IEEE Antenna Wireless Propag. Lett.*, vol. 17, no. 2, pp. 287–290, Feb. 2018.

[21] T. Dinc and H. Krishnaswamy, "A T/R antenna pair with polarization-based reconfigurable wideband self-interference cancellation for simultaneous transmit and receive," in *IEEE MTT-S Int. Microw. Symp. Dig.*, May 2015, pp. 1–4.

[22] X. Wang, W. Che, W. Yang, W. Feng, and L. Gu, "Self-interference cancellation antenna using auxiliary port reflection for full-duplex application," *IEEE Antennas Wireless Compon. Lett.*, vol. 16, pp. 2873–2876, 2017.

[23] E. Tsakalaki, O. N. Alrabadi, A. Tatomirescu, E. de Carvalho, and G. F. Perdersen, "Concurrent communication and sensing in cognitive radio devices: Challenges and an enabling solution," *IEEE Trans. Antennas Propag.*, vol. 62, no. 3, pp. 1125–1137, Mar. 2014.

[24] O. N. Alrabadi, A. Tatomirescu, M. B. Knudsen, M. Pelosi, and G. F. Pedersen, "Breaking the transmitter–receiver isolation barrier in mobile handsets with spatial duplexing," *IEEE Trans. Antenna Propag.*, vol. 61, no. 4, pp. 2241–2251, Apr. 2013.

[25] H. Qi, L. Liu, X. Yin, H. Zhao, and W. J. Kulesza, "Mutual coupling suppression between two closely spaced microstrip antennas with an asymmetrical coplanar strip wall," *IEEE Antenna Propag. Lett.*, vol. 15, pp. 191–194, 2016.

[26] H. Qi, X. Yin, L. Liu, Y. Rong, and H. Qian, "Improving isolation between closely spaced patch antennas using interdigital lines," *IEEE Antennas Wireless Propag. Lett.*, vol. 15, pp. 286–289, 2015.

[27] K. E. Kolodziej, P. T. Hurst, A. J. Fenn, and L. I. Parad, "Ring array antenna with optimized beamformer for simultaneous transmit and receive," in *Proc. IEEE Int. Symp. Antennas Propag.*, Chicago, IL, USA, Jul. 2012, pp. 1–2.

[28] T. J. Douglas and K. Sarabandi, "A high-isolation two-port planar antenna system for communication and radar applications," *IEEE Access*, vol. 6, pp. 9951–9959, 2018.

[29] H. Makimura, K. Nishimoto, T. Yanagi, T. Fukasama, and H. Miyashita, "Novel decoupling concept for strongly coupled frequency-dependent antenna arrays," *IEEE Trans. Antenna Propag.*, vol. 65, no. 10, pp. 5147–5154, Oct. 2017.

GIRDHARI CHAUDHARY (S'10–M'13) received the B.E. degree in electronics and communication engineering from Nepal Engineering College (NEC), Kathmandu, Nepal, in 2004, the M.Tech. degree in electronics and communication engineering from MNIT, Jaipur, India, in 2007, and the Ph.D. degree in electronics engineering from Chonbuk National University, South Korea, in 2013.

He worked as a Principal Investigator (PI) of the Independent Project through the Basic Science Research Program of the National Research Foundation (NRF), funded by the Ministry of Education, South Korea. He is currently an Assistant Research Professor with the Division of Electronics Engineering, Chonbuk National University, South Korea. His research interests include multi-band tunable passive circuits, negative group delay circuits and its applications, in-band full duplex systems, and high efficiency power amplifiers.

Dr. Chaudhary is a recipient of the BK21 PLUS Research Excellence Award 2015 from the Ministry of Education, South Korea. He has currently received the Korean Research Fellowship (KRF) through the National Research Foundation (NRF) of Korea, funded by the Ministry of Science and ICT. He has served as a Reviewer for the IEEE TRANSACTION ON MICROWAVE THEORY AND TECHNIQUES, the IEEE MICROWAVE AND WIRELESS COMPONENT LETTERS, the IEEE TRANSACTION ON CIRCUIT AND SYSTEMS-I, and the IEEE TRANSACTION ON INDUSTRIAL ELECTRONICS.

JUNHYUNG JEONG (S'13) received the B.E. degree in electronics and information engineering from Chonbuk National University, Jollabuk-do, South Korea, in 2012, and the M.E. degree in electronics engineering from Chonbuk National University, in 2014, where he is currently pursuing the Ph.D. degree with the Division of Electronics Engineering. His research interests include RF filter, high-efficiency power amplifiers, and RF transmitter.

YONGCHAE JEONG (M'99–SM'10) received the B.S.E.E., M.S.E.E., and Ph.D. degrees in electronics engineering from Sogang University, Seoul, South Korea, in 1989, 1991, and 1996, respectively.

From 1991 to 1998, he worked as a Senior Engineer with Samsung Electronics. In 1998, he joined the Division of Electronics Engineering, Chonbuk National University, Jeonju, South Korea. From 2006 to 2007, he was with the Georgia Institute of Technology, as a Visiting Professor. He is currently a Professor, director of the IT Convergence Research Center, and the Director of the HOPE-IT Human Resource Development Center of BK21 PLUS, Chonbuk National University. He has authored and coauthored over 230 papers in international journals and conference proceeding. He is currently teaching and conducting research in the area of microwave passive and active circuits, mobile and satellite base-station RF systems, design of periodic defected transmission line, negative group delay circuits and its applications, in-band full duplex radio, and RFIC design. He is a member of the Korea Institute of Electromagnetic Engineering and Science (KIEES).

• • •